

Coupling between small polarons and ferroelectricity in BaTiO₃

Darin Joseph

Dipartimento di Fisica e Astronomia, Università di Bologna, 40127 Bologna, Italy

Cesare Franchini

*University of Vienna, Faculty of Physics, Center for Computational Materials Science, Vienna, Austria and
Dipartimento di Fisica e Astronomia, Università di Bologna, 40127 Bologna, Italy*

(Dated: March 18, 2025)

In this study, we investigate the formation of electron and hole small polarons in the prototypical ferroelectric material BaTiO₃, with a focus on their interaction with ferroelectric distortive fields. To accurately describe the ferroelectric phase in electronically correlated BaTiO₃, we employ the HSE06 hybrid functional, which addresses the limitations of conventional DFT and DFT+U models, providing a more precise depiction of both ferroelectric and polaronic behaviors. Our analysis spans three structural phases of BaTiO₃: cubic, tetragonal, and orthorhombic. We uncover a unique phase-dependent trend in electron polaron stability, which progressively increases across the structural phases, peaking in the rhombohedral phase due to the constructive coupling between the polaron and ferroelectric phonon fields. In contrast, hole polarons exhibit a stability pattern largely unaffected by the phase transitions. Furthermore, we observe that polaron self-trapping significantly alters the local ferroelectric distortive pattern, which propagates to neighboring sites but has a minimal effect on the long-range macroscopic spontaneous polarization. Charge trapping is also associated with localized spin formation, opening new possibilities for enhanced functionalities in multiferroic materials.

I. INTRODUCTION

Marked by a spontaneous electric polarization that can be reversed by an external electric field, ferroelectric (FE) materials are vital in a wide range of technological applications [1–4]. Capitalizing on this unique switchable polarization property, their applications range from capacitors and transducers to non-volatile memory devices [5–7]. Due to its impressive FE properties, Barium titanate (BaTiO₃) has been the subject of exhaustive research [8, 9]. This also includes significant attention to understanding the impact of localized states, such as those induced by defects, on its FE behaviour.

FE behaviour and dielectric properties are altered due to the presence of defects that introduce localized electronic states within the band structure. In perovskites such as BaTiO₃ and ZrPtO₄, the presence of oxygen vacancies act as electron donors, potentially creating defect dipoles that pin domain walls and thereby impacting polarization switching [10–13]. Other studies show that ferroelectricity decreases due to cation vacancies, such as titanium vacancies in BaTiO₃ [14, 15]. Similarly, for SrTiO₃, intrinsic defects like antisite titanium induce local polarization and lead to the formation of polar nanoregions [16–18]. Furthermore, studies also reveal that the introduction of foreign ions into YFeO₃ or HfO₂ can modify FE properties by distortions in the lattice, alterations in electronic structure or formation of new defect complexes [19–21].

Similarly, the formation of polarons likewise results in the localized state within the band structure. Unlike defects, which are associated with ionic or atomic anomalies, polarons are quasiparticles that form as a result of interaction between charge carriers and lattice

vibrations (phonons) [22–25]. Based on the extent of electron-phonon coupling, polarons are usually classified into large and small polarons, with small polarons showing strong coupling and localized behaviour [25–27]. Polaron signatures have been detected in several materials such as transition-metal oxides, organic semiconductors, polymers, manganites, hybrid perovskites, cuprites, magnetic semiconductors, and 2D materials, to name a few [28–42]. Charge transport, colossal magnetoresistance, photoemission, surface reactivity, thermoelectricity and (multi)ferroism are a few physical phenomena where polaron-mediated effects play a crucial role [33, 38, 43–49].

In FE perovskites such as PbTiO₃, theoretical studies have shown that electron polarons become self-trapped and thereby influence the n-type conductivity of the material [50]. Experimental indications that are linked to the material’s optical and transport properties have long suggested the presence and impact of small polarons in BaTiO₃. For instance, in BaTiO₃ single crystals, the characteristic green luminescence has been linked to small polarons [51, 52]. Furthermore, a proposed explanation for the transport behaviour of charged carriers in BaTiO₃ is the concept of a hopping mechanism involving small polarons [53–56]. Insights into the existence and stability of polarons in BaTiO₃ have further been provided by theoretical studies. Computational investigation using Heyd-Scuseria-Ernzerhof (HSE06) functional shows that hole polarons can self-trap in BaTiO₃, preferentially localizing on oxygen atoms in both tetragonal and cubic phases [57]. The studies link the experimentally observed low-temperature photoluminescence to the calculated emission peak energy from the recombination of a conduction band electron with a self-trapped hole

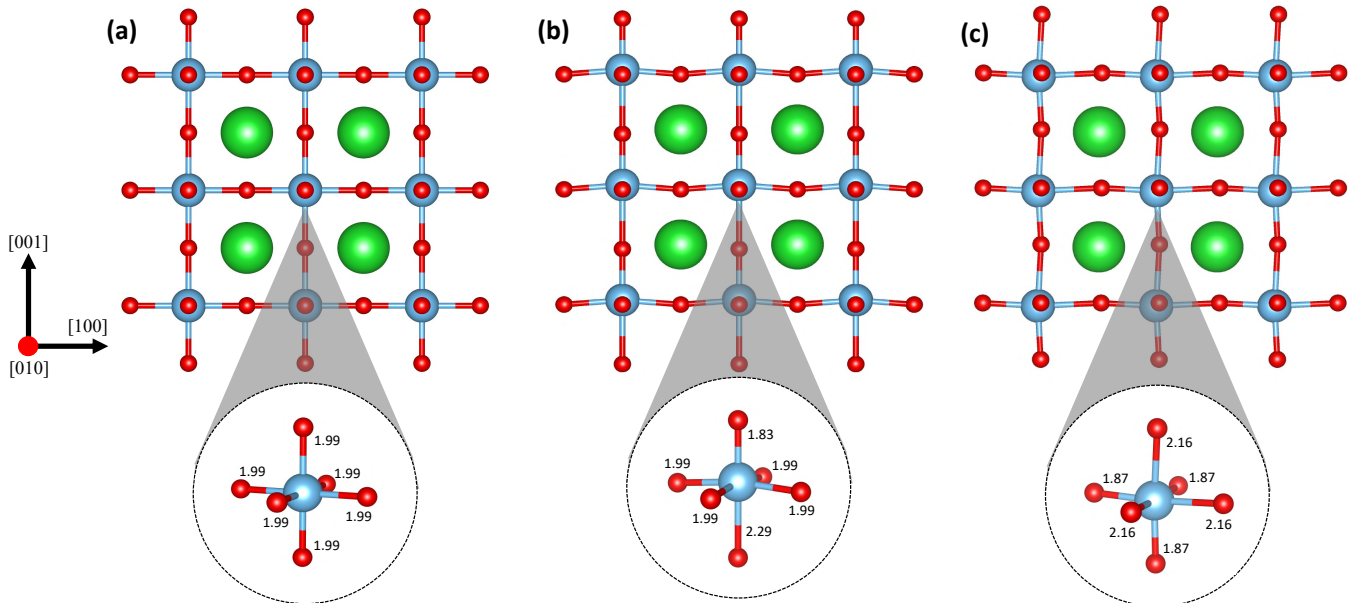


Figure 1. (a) Cubic BaTiO₃ with zero Ti off-centering (b) Tetragonal BaTiO₃ with Ti off-centering in [001] direction and (c) Rhombohedral BaTiO₃ with Ti off-centering in the [111] direction.

polaron. Similarly, DFT+U studies also confirm the stability of hole polarons in BaTiO₃'s cubic phase [58].

A unique opportunity to explore novel functionalities in materials is presented by understanding the interplay between FE order and small polarons, gaining insight into whether and how FE distortions (δ_{Fe}) can favor or disfavor polaron formation. FE polarons result from such a constructive interplay and are described as polarons stabilized by FE distortions. The presence of FE large polarons in halide perovskites is found to improve charge transport efficiency and enhance performance in optical applications such as solar cells and light-emitting devices [48, 49]. Furthermore, research has demonstrated the role of polarons in the emergence of polarization in SrTiO₃ and CaTiO₃ [16, 59]. Moreover, ongoing studies are examining multiferroism induced via small polaron dynamics in BaTiO₃ [60, 61].

Despite the available results and knowledge, the interplay between ferroelectricity and small polarons in BaTiO₃ remains a topic that requires a deeper analysis. There is a limited number of literature and a detailed investigation needs to be done to get a clearer picture of the mutual influence of these phenomena. In particular, the impact of ferroelectricity on hole polarons in different phases of BaTiO₃ remains an unexplored domain. The inaccuracy of DFT+U in capturing the δ_{Fe} complicates the theoretical investigation, since this method is used mostly to study polarons in materials [62, 63].

The main aim of this study is to fill this gap by investigating the formation of electron and hole polarons in three different phases of BaTiO₃ using hybrid functionals. The stability of polarons in a localized state is compared to its delocalized counterpart across the cubic, tetragonal

and rhombohedral polymorphs of BaTiO₃ (see Fig. 1). The analysis of the variation of polaron formation energy across the different structures and the reciprocal impact of polarons on the δ_{Fe} , which here is attributed to the relative displacement of Ti and O atoms, is the major component of the current study. Our research elucidates the complex interplay between ferroelectricity and small polarons by comparing the effects of electron and hole polarons on the FE distortive field and polarization in BaTiO₃.

II. METHODS

Density Functional Theory (DFT) stands as a powerful tool in the electronic structures calculations [64, 65]. While this is the case, the limitations of DFT are not unfamiliar, especially when it comes to the study of polarons [66, 67]. For modelling systems where electron localization is pivotal, DFT often leads to inaccuracies due to their inherent self-interaction errors. The widely adopted approach to address this issue is the integration of the Hubbard U term [68]. The description of localized charge carriers are enhanced with DFT+U method by adding an on-site coulombic interaction and thereby correcting the self-interaction errors [69].

However, DFT+U posed a challenge to the current study. The stabilization of δ_{Fe} within the FE systems plays a vital role in the study. But a linear reduction in δ_{Fe} was observed for the FE phases of BaTiO₃ as the U value is increased from 0 to 5 eV and beyond, resulting in a paraelectric cubic structure [62, 63]. Such an observation was evident for both tetragonal and rhombohedral

phases during the geometrical optimization. Stronger localization of electrons in the d -orbitals of the Ti atoms arises with the increase in the U value, consequentially diminishing the covalency due to a suppressed hybridization between the O $2p$ and Ti $3d$ orbitals. Figure 2 illustrates the phonon-dispersion curve of cubic BaTiO₃ and clearly demonstrates how PBE+ U method does not show any imaginary phonon modes. The absence of these modes indicate that the cubic BaTiO₃ does not exhibit soft phonon modes associated with FE instability. This disability of DFT+ U to stabilize the δ_{Fe} , have already been reported and studied[62, 63]

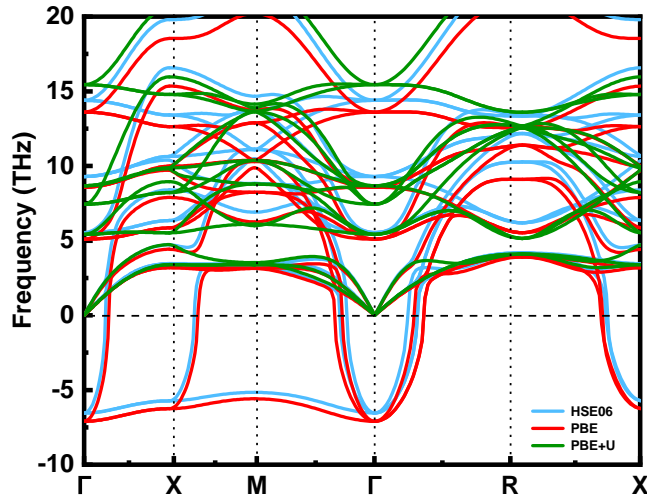


Figure 2. Phonon dispersion curve of cubic BaTiO₃ plotted with HSE06, PBE and PBE+ U . With PBE+ U , for a U value of 6 eV, a clear vanishing of imaginary modes are observed. This depicts the effect of Hubbard U parameter in suppressing the δ_{Fe} in the system.

An alternative approach to overcome this limitation was to utilize the hybrid functionals [70]. Specifically, we adopted the HSE06 formalism [71]. The fraction of exact Hartree-Fock exchange was set to the standard value of $\alpha = 0.25$. The first-principles calculations were carried out using the Vienna Ab initio Simulation Package (VASP) in combination with the Projector Augmented Wave (PAW) approach [72–75]. A plane wave energy cut-off of 320 eV was utilized in all calculations, with 10^{-5} eV set as the convergence threshold of the electronic self-consistency. The polaronic systems were modelled with a $3 \times 3 \times 3$ supercell, containing 135 atoms. The structural relaxation of the ionic positions was continued until the Hellman-Feynman forces were lower than 0.01 eV/\AA , and a $2 \times 2 \times 2$ Monkhorst-Pack k -point mesh was utilized for the Brillouin zone integration. Employing HSE06 for lattice relaxations stabilized the δ_{Fe} within the ferroelectric systems and concurrently provided lattice parameters and band gaps that more closely agreed to the experimental values[8, 76, 77].

For the formation of electron polarons, an extra electron was introduced into the system and conversely for

formation of hole polarons, an electron was removed. Initially, the result was a delocalised solution but by manually breaking the symmetry, it was possible to localize the electron and hole on the preferred site. For electron polarons, six Ti-O bonds around the desired Ti atom was extended, while for hole polarons, two Ti-O bonds next to the chosen O atom was extended. The polaronic formation energy was calculated using the following formula:

$$E_{POL} = E_{dist}^{loc} - E_{unif}^{deloc} \quad (1)$$

where (E_{dist}^{loc}) is the total energy of the supercell with a polaron, (E_{unif}^{deloc}) is the total energy of the pristine supercell with the extra charge delocalized in the entire crystal (no polaron). This formula allows us to calculate the energy gain of forming a polaron in the material as compared to a delocalized uniform solution [25].

Berry-phase approach within the modern theory of polarization was employed to calculate the ferroelectric polarization of both the pristine and polaronic ferroelectric systems [4, 78]. Within the Berry phase approach, the spontaneous polarization is computed by considering the polarization difference between the ferroelectric phase and a centrosymmetric reference phase, which is the cubic BaTiO₃ in the present study. In the context of polaron systems, the considered reference system was a cubic BaTiO₃ with a localized charge carrier.

III. RESULTS

A. Polarons : Electrons and Hole Polarons in BaTiO₃

In this section, we inspect the formation of small electron and hole polaron in three polymorphs of BaTiO₃ - cubic, tetragonal, and rhombohedral. The distinction among these polymorphs is marked by a varying degree of Ti off-centering within the crystal structure, which shows a progressive increase as we transition from cubic to tetragonal and finally to the rhombohedral, as depicted in Fig.1. The cubic phase of BaTiO₃ has a perfectly centered Ti and O atoms, possessing zero off-centering, while the ferroelectric tetragonal and rhombohedral phases are characterized by a Ti off-centering along [001] and [111] directions respectively, leading to δ_{Fe} in the systems. For the tetragonal phase, we calculate this δ_{Fe} to be 0.16 \AA along the [001] direction, while for the rhombohedral phase, the δ_{Fe} is computed to be 0.10 \AA along the [111] direction. The crystal symmetry and its characteristic FE distortive field play a critical role in the formation and properties of the polaron.

Analysis of the charge density plots confirmed the formation of small polarons and the spatial distribution of charge. For electron polarons, a Ti-3d orbital character was exhibited across all three polymorphs, as shown in Fig.3, while an O-2p orbital character was exhibited for

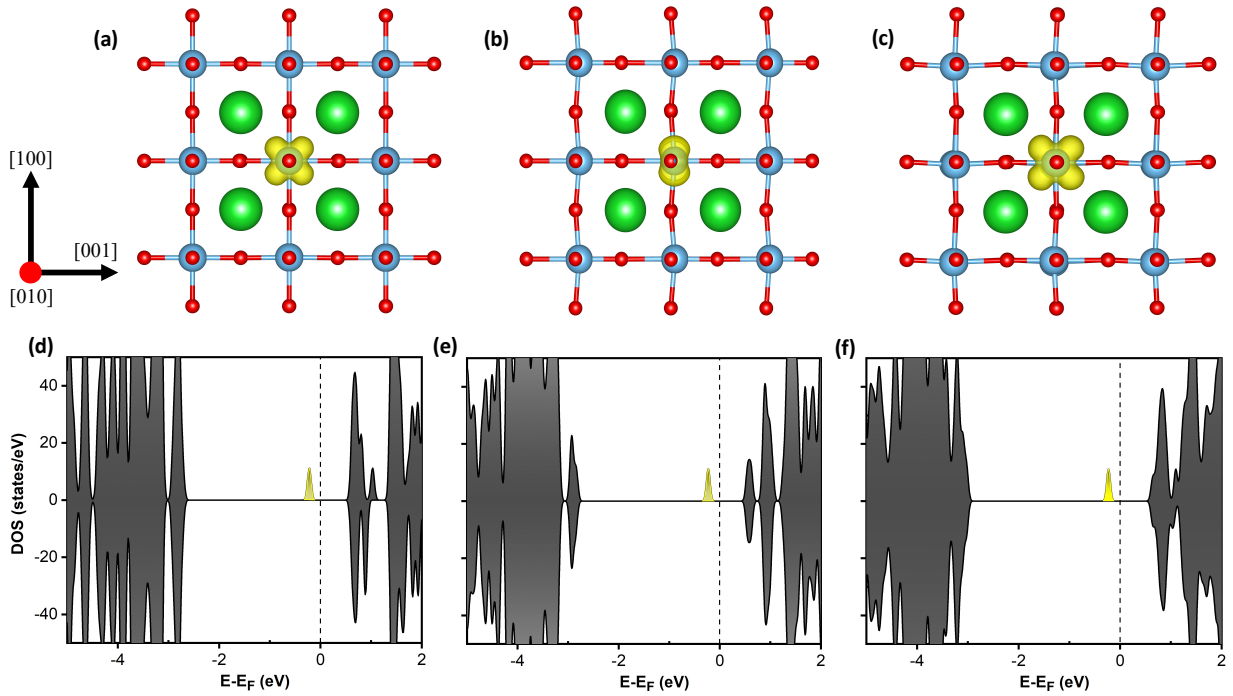


Figure 3. The charge density plots due to formation of electron polaron on (a) Cubic BaTiO₃ (b) Tetragonal BaTiO₃ (c) Rhombohedral BaTiO₃. The density of states and the formation of an in-gap state is depicted for (d) Cubic BaTiO₃ (e) Tetragonal BaTiO₃ (f) Rhombohedral BaTiO₃.

hole polarons in all three polymorphs, as shown in Fig.4. For the electron polarons in the cubic and rhombohedral phases, we observed the d_{xz} orbital character, while the preferential occupation of the extra electron in the tetragonal phase was the d_{xy} orbital. For hole polarons, we observed an admixture of p_y and p_z orbital character for both cubic phase, a p_y orbital character for tetragonal phases, while a p_z orbital character was observed for the rhombohedral phase of BaTiO₃.

Further insights on polaron stability can be obtained from the dependence of E_{POL} on the crystal symmetry. The stability of electron polarons in BaTiO₃ exhibits a clear trend with crystal symmetry, increasing from cubic to tetragonal to rhombohedral phases as shown in Fig. 5. This can be attributed to two reasons: first, the level of antibonding hybridization between the Ti-3d and O-2p orbitals at the conduction band minimum and second, the degree of Ti off-centering. The rhombohedral BaTiO₃ exhibits an E_{POL} of -0.26 eV, which is the lowest of all the three phases considered. The cubic and tetragonal phases show an E_{POL} of -0.07 eV and -0.11 eV respectively, clearly showing how rhombohedral phase outperforms the other two phases. As mentioned previously, this is attributed to the strong anti-bonding hybridization in this phase, thus allowing maximum energy release upon electron localization on the Ti-3d orbital. A large electronic gain energy (E_{EL}) of -0.49 eV compared to the tetragonal phases' -0.32 eV validates this. The decrease in δ_{Fe} of the polaronic octahedron is more significant for the rhombohedral phase than for the tetragonal phase

(discussed in detail in the next section), which further validates our observation because the δ_{Fe} in BaTiO₃ is strongly associated with the hybridization between Ti-3d and O-2p. Furthermore, the ferroelectric tetragonal and rhombohedral phases, because they already possess off-centering, require less energy to distort compared to the cubic phase. This is clear from the structural energy cost (E_{ST}), which is calculated to be 0.27 eV from cubic, while for the tetragonal and rhombohedral phase, this is calculated to be 0.23 eV. These results align with previous findings by Tsunoda et al., highlighting the importance of anti-bonding hybridisation and local displacement of Ti ions along the [111] direction in both rhombohedral BaTiO₃ and structurally disordered cubic phases for stabilizing self-trapped polarons. [60]

Interestingly, this trend is not exactly mimicked by hole polarons, as they are already evidently stable in all three polymorphs. Polaron formation energies of -0.20 eV, -0.22 eV, and -0.25 eV are recorded for cubic, tetragonal and rhombohedral BaTiO₃, respectively. Although the trend of an increase in stability as one transitions from cubic to rhombohedral is also observed for the hole polaron system, the differences are modest, as shown in Fig.5. Unlike electron polarons, holes are localized on O-2p bonding orbitals, and stabilization involves weakening the bonding O-2p and Ti-3d hybrids. Because the bonding states are already lower in energy and more stable, the hole-polaron formation results in a lower energy gain and smaller variations in the hole-polaron stability. Symmetry also plays a smaller

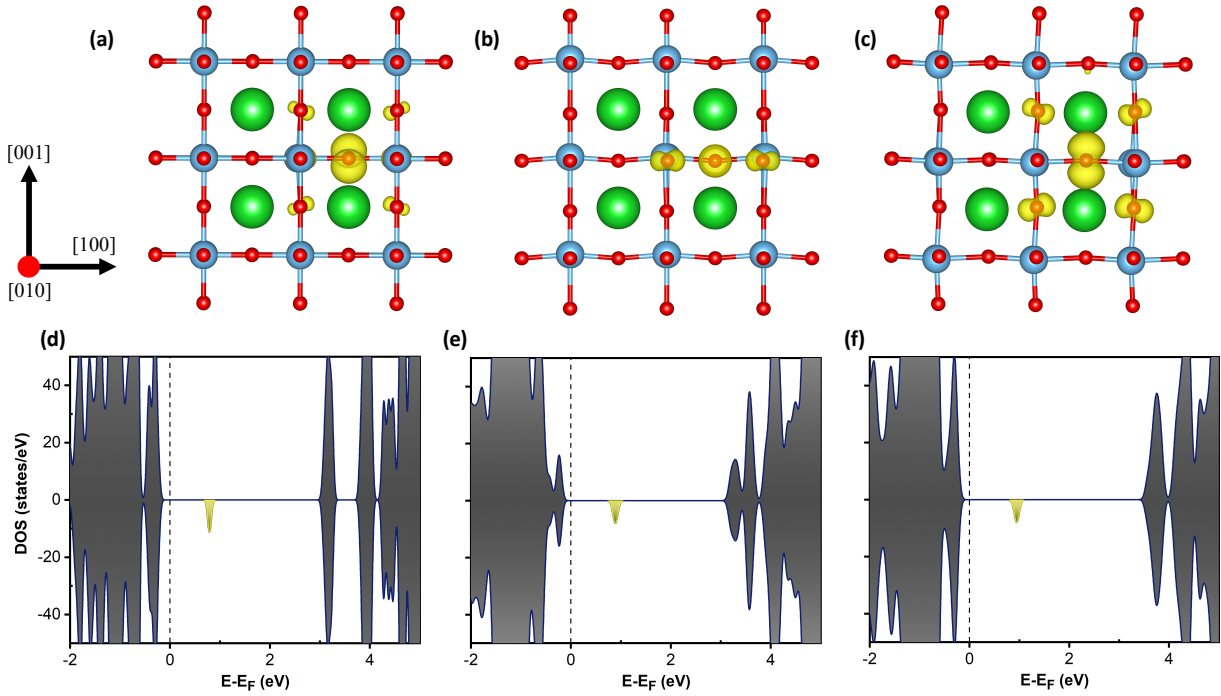


Figure 4. The charge density plots due to formation of hole polaron on (a) Cubic BaTiO₃ (b) Tetragonal BaTiO₃ (c) Rhombohedral BaTiO₃. The density of states and the formation of an in-gap state is depicted for (d) Cubic BaTiO₃ (e) Tetragonal BaTiO₃ (f) Rhombohedral BaTiO₃.

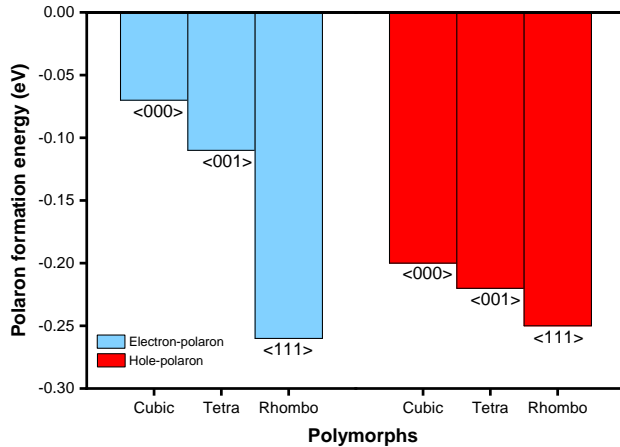


Figure 5. The comparison of polaron formation energy for different phases of BaTiO₃ for both the electron and hole polaron. The figure depicts the enhanced stability of electron polaron for rhombohedral phase, while the same is not observed in the case of hole polaron, indicating the effect of [111] off-centering of Ti atom in stabilizing the polaron.

role in the case of hole polarons because the distortion of the O atom, on which the hole polaron forms, from its centrosymmetric position in the ferroelectric phases is computed to be approximately 90% less than that of Ti distortion. The combined effect could possibly

explain why a small phase-dependent variation in E_{POL} was observed in the case of hole polarons. The slight increase in E_{POL} can be attributed to the pre-distorted TiO₆ octahedron in the ferroelectric phases, which could slightly ease the relaxation of the O-site.

Because we now understand the factors that affect the stability of polarons in the material, it is essential to examine the resulting structural distortions introduced by localized charge carriers. Substantial structural distortions were observed due to the formation of polarons and they displayed variations based on the type of polaron and the BaTiO₃ polymorph.

In cubic BaTiO₃, the formation of an electron polaron is accompanied by an equal increase in the Ti-O bond lengths around the polaronic sites. The elongation of the Ti-O bonds around the polaronic site was approximately 3%. As a result of this increase, we also observed a corresponding decrease in the bond length between the O atoms in the polaronic octahedron and the first nearest neighbor (1NN) Ti atoms. We compute the decrease to be uniform for all such bonds, and is determined to be approximately 3.5%. As shown in Fig1(b), the in-plane bonds of tetragonal BaTiO₃ are equal in length, whereas the out-of-plane bonds are of two different lengths, one short and the other long. As a polaron forms in this crystal symmetry, we observed an enhancement in the Ti-O in-plane bond lengths in the polaronic unit cell, which was computed to be 3%.

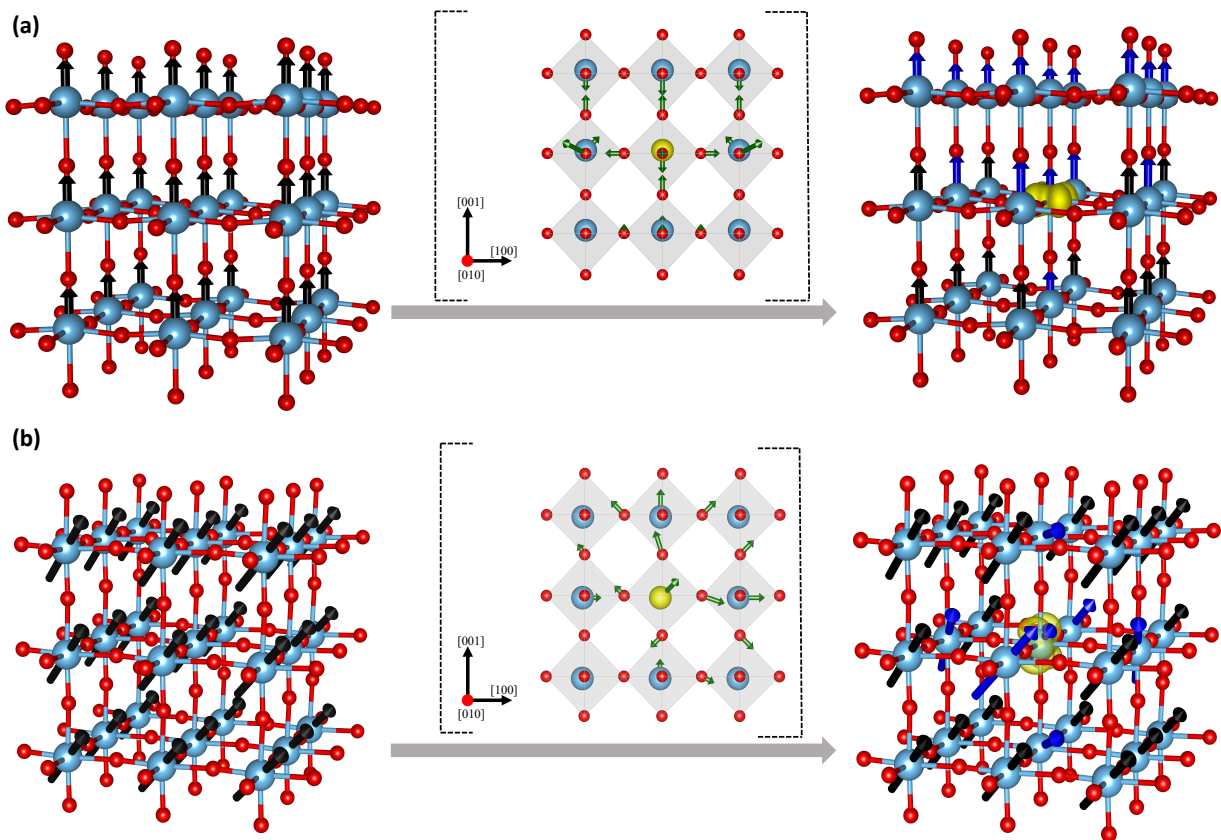


Figure 6. The figure represents a schematic depiction of the evolution of δ_{Fe} from a pristine to polaronic state as an electron localizes on a Ti atom in the (a) tetragonal and (b) rhombohedral phases of BaTiO_3 . The blue arrows in the figures on the right indicate the ferroelectric distortions, which vary in both magnitude and direction compared to the δ_{Fe} in the pristine state, represented by black arrows. These transformations in the δ_{Fe} are attributed to the polaronic distortions, as represented in square brackets. Here, the atom represented in yellow colour is the polaronic site and the green arrows represent the polaronic distortion.

However, for out-of-plane bonds, we observed that the shorter bond experienced a considerable increment of 2%, whereas a decrease of 1% was observed for the longer bond. The rhombohedral phase of BaTiO_3 has two distinct bond types according to its length, three of which are longer and the other three are shorter, as shown in Fig1(c). The presence of polarons induced all three longer bonds to contract by approximately 2%, whereas all shorter bonds showed a significant elongation of approximately 8% in the polaronic site. We observed that these polaronic distortions also propagated beyond the immediate vicinity of the polaron; however, their significance gradually decreased with distance. The polaronic distortions affect the δ_{Fe} , where the sites that underwent major polaronic distortions exhibited significant changes to δ_{Fe} as well. Hence, significant changes in δ_{Fe} were observed near the polaron relative to the sites farther away. Section B provides a more comprehensive discussion of the influence of electron polarons on the δ_{Fe} and properties throughout the system.

For hole polarons, the structural distortions showed slight variations compared to their electron-polaron counterparts. The bonds between the Ti atoms and polaronic O atom showed an increase in the bond length by approximately 6% for cubic BaTiO_3 . As a consequence of this shift of the 1NN Ti atoms, other Ti-O bonds in TiO_6 octahedrons decreased, with a significant decrease of 5.5% only observed for the in-plane bond along the [100] direction. Similarly, the observations are mimicked in tetragonal BaTiO_3 as a hole polaron is formed. Upon the formation of hole polarons, the length of the two bonds between the polaronic O atom and the two nearest-neighbor Ti atoms increased by approximately 4%. As a result of this increase, we observed that the other in-plane Ti-O bonds for the two neighboring octahedrons decreased in length. A significant decrease of approximately 4% is observed for one of the bonds in the [100] direction. This also results in a δ_{Fe} in the [010] direction on both 1NN TiO_6 octahedrons, but the dipole moment cancels it out because they are equal and opposite. The presence of a hole polaron in the rhombohedral phase of BaTiO_3 shows a similar trend;

however, the elongations of the two bonds around the O atom are unequal. While one bond showed a negligible change, the other bond experienced a significant increase in length. Similar to the case with electron polarons, polaronic distortion is also observed at sites farther from the polaron, but with lesser significance relative to the nearest neighboring sites. All these polaronic distortions affect δ_{Fe} as mentioned before and this correlated effect of hole polarons on the ferroelectricity throughout the system is further discussed in section C.

B. Effect of electron polarons on the ferroelectric properties

The previous section discussed the influence of ferroelectricity on the formation and characteristics of the polarons. In the current section, the focus is on the reciprocal effect, that is, the impact of electron polarons on the ferroelectric properties of the tetragonal and rhombohedral phases of BaTiO₃.

In tetragonal BaTiO₃, the Ti atoms exist in a distorted octahedral environment with C_{4v} symmetry. As discussed in the previous section, the self-trapping of an extra electron at the Ti site leads to significant changes in the local structure, primarily affecting the polaronic site. The electron localizes in the d_{xy} orbital, increasing the electron density in the xy plane and causing stronger electron-electron repulsion with the in-plane O atoms. The in-plane Ti-O bonds elongate as a result of this repulsion. Concurrently, the redistribution of electron density leads to reduced hybridization between the polaronic Ti atom and the out-of-plane O atoms, which weakens the out-of-plane Ti-O bonds. As a result, we observed that the polaronic Ti atom shifted towards the center of the octahedron by 0.014 Å, whereas all the in-plane oxygen atoms shifted away from the Ti atom by approximately 0.07 Å. The distortions are schematically represented in the Fig.6(a). There was also a noticeable shift in both the out-of-plane O atoms by approximately 0.02 Å in the [001] direction. All these shifts result in changes in the bond lengths, as discussed Section A. The weakened hybridization between the Ti-3d and O-2p orbitals reduces the covalent character of the Ti-O bonds, decreasing the δ_{Fe} in the polaronic octahedron by approximately 15% and pushing the unit cell towards a more cubic-like shape.

For the other TiO₆ octahedrons in the x-y plane containing the polaron, we observed a modest increase in the δ_{Fe} , with an increase of approximately 2% for the 1NN TiO₆ octahedrons in the [100], $[\bar{1}00]$, [010] and $[0\bar{1}0]$ directions. This can be attributed to the shift of in-plane oxygen away from the polaronic Ti atom. The neighboring octahedrons accommodated such shifts by shrinking one of their in-plane bonds (the Ti-O bond connecting Ti and the shifted O of the polaronic octahedron) by 4%. Consequently, the Ti atom in all these 1NN octahedrons shifted further away from its centrosymmetric position by 0.01 Å. Simultaneously, the out-of-plane O atoms in the

same octahedrons experienced minimal shifts to stabilize the octahedrons that were distorted owing to the shrinking of the in-plane bond. For the octahedrons in the x-y plane above the polaronic octahedron, we observed a decrease in δ_{Fe} . This decrease progressively became less significant as we moved farther away from the polaronic site. A significant decrease of approximately 14% was computed for the 1NN octahedron in the [001] direction, whereas for the other sites in the same plane, the decrease was approximately 5%-8%. This can be attributed to the distortion of the out-of-plane O atom of the polaronic octahedron in the [001] direction, which results in the shortening of the longer bond of the 1NN octahedron above it. During the same time, the Ti atom in the same octahedron shifted down (that is, the direction $[00\bar{1}]$) by 0.02 Å, resulting in a significant decrease in the δ_{Fe} for this particular site. Ti shift was minimal for other sites in the same plane, which accounts for the negligible changes to the δ_{Fe} . Interestingly, for the sites in the x-y plane below the polaronic octahedron, we observed little to no change in δ_{Fe} . This could be due to the minimal spread of polaronic distortions in this plane owing to less susceptibility to changes since it lies in the opposite direction to the [001] tetragonal distortion in the system. However, owing to the shift in the out-of-plane O atom of the polaronic octahedron in the [001] direction, we observed an elongation of the shorter out-of-plane bond of the octahedron below the polaron. During the same time, the Ti and in-plane O atoms also shifted in the [001] direction, resulting in an overall decrease of 2% in δ_{Fe} at this site. The distortion of 0.009 Å of the Ti and O atoms is minimal in the $[00\bar{1}]$ 1NN octahedron compared to that in the [001] 1NN octahedron; hence, the observed changes to the ferroelectricity of this specific site and the others in the same plane are negligible. In summary, the variations in the δ_{Fe} exhibited planar dependency, where we clearly observed a modest increase in the x-y plane containing polarons, except for the polaronic site. For sites above this plane, there was a noticeable decrease in the δ_{Fe} , whereas for sites below this plane, there was a negligible decrease in the δ_{Fe} . All these conclusions are based on the results obtained with a 3x3x3 supercell.

Upon the formation of electron polaron, the rhombohedral phase of BaTiO₃ shows a similar trend as observed in tetragonal BaTiO₃ but the reduction in δ_{Fe} is more pronounced. A substantial decrease of approximately 68% in δ_{Fe} was observed in all directions [111]. Such a decrease is the consequence of polaronic distortions, which result in a shift of the Ti atom towards its centrosymmetric position by 0.06 Å. In addition, an interesting pattern was observed for the distortions of O atoms around the polaron: the pronounced shift of O atoms in the x-direction of the octahedrons was only along the x-direction, whereas the O atoms in the y- and z-directions of the octahedron showed a similar trend of significantly shifting only along the y- and z-directions, respectively, as shown in Fig6(b). Furthermore, an asymmetric distortion, with the O atoms on either side of the polaronic Ti atom dis-

torting non-uniformly, was observed. Specifically, a significant shift of 0.09 \AA was noted for the O atoms in the [100], [010], and [001] directions, whereas a minimal shift of 0.01 \AA was exhibited by the O atoms in the $[\bar{1}00]$, $[0\bar{1}0]$ and $[00\bar{1}]$ directions. As there is already an existing [111] polarization in this phase of BaTiO_3 , the O atoms in the direction of the polarization are more prone to distortions than those in the direction opposite to the polarization. The changes in bond lengths upon polaron formation, as discussed in the Section A, can be attributed to these polaronic shifts. The Ti site holding a C_{3v} site symmetry in rhombohedral phase creates anti-bonding states with the neighboring O-2p orbitals at the conduction band minimum. As discussed in Tsunoda et al.'s paper, electron localization on a Ti-3d orbital modifies the TiO_6 octahedra such that it reduces this anti-bonding hybridization with the neighboring O-2p orbitals [60]. This observation was also similar in our calculations, and given that such reduced hybridization indicates reduced ferroelectricity for BaTiO_3 , this can explain the significant reduction in δ_{Fe} observed in the polaronic octahedron. The δ_{Fe} values of the neighboring sites were also affected by the polaronic distortions described earlier. For the octahedron in the [100] direction, a 0.06 \AA shift of the Ti atom towards its centrosymmetric position in the x-direction was observed. This combined with the distortion of the O atom in the [100] direction of the polaronic octahedron, resulted in the shrinking of the longer bond (only in the [100] direction) by approximately 0.16 \AA for this specific octahedron. Overall, a 85% decrease in δ_{Fe} in the x-direction was observed, whereas distortions along the y- and z-directions did not exhibit any variation. Furthermore, the polaronic distortions and the consequent changes to δ_{Fe} are significantly reduced with increasing distance from the polaron. The nearest neighbors in the [010] and [001] directions displayed a pattern analogous to that of the [100] nearest neighbor, with a 85% reduction in δ_{Fe} along the y- and z-directions, respectively. This can also be attributed to the polaronic distortions that resulted in the Ti atoms in the respective octahedrons shifting towards the centrosymmetric position by 0.06 \AA only along the respective direction, and the directional shift of O atom in the polaronic octahedron, as described earlier. Minimal shifts of atoms present in the $[\bar{1}00]$, $[0\bar{1}0]$ and $[00\bar{1}]$ directions resulted in a less pronounced reduction of 33% to δ_{Fe} across these sites.

We further inspected the effect of small-polaron formation on spontaneous polarization (P_s) using the modern theory of polarization. During these calculations, we only considered the lattice effect due to polaron formation. As expected from the localized nature of the polaron-induced distortive pattern, P_s for the polaronic tetragonal BaTiO_3 (0.38 C/cm^2) remains close to the value of pristine BaTiO_3 , as tabulated in Table I. Moreover, the energy difference between the ferroelectric and paraelectric polaronic phases was calculated as 0.032 eV/f.u. , which is comparable to the energy difference of 0.03 eV/f.u. for the pristine BaTiO_3 systems. Similarly, in

Table I. Polarization values (in C/m^2) for different structural phases (Cubic, Tetragonal, and Rhombohedral) of BaTiO_3 . The table also compares the effect of electron and hole polaron formation on the macroscopic polarization in each phase.

	Cubic	Tetragonal	Rhombohedral
Pristine	0	0.39	0.45
Electron Polaron	0	0.38	0.4
Hole Polaron	0	0.395	0.46

the rhombohedral phase, the calculated P_s reduces to 0.4 C/cm^2 for the polaronic state, compared to the pristine state, as tabulated in Table I. In addition, an energy difference of 0.048 eV/f.u. in the polaronic state is comparable to 0.044 eV/f.u. in the pristine BaTiO_3 . The studies unveils the co-existence of δ_{Fe} and polaronic distortions, thereby revealing the formation of ferroelectric electron polarons in the material. While the self-trapping of electron polarons lead to a slight reduction in the ferroelectric properties of both the ferroelectric phases, their impact is not strong enough to completely suppress the overall ferroelectricity in the systems. The self-trapping of electron polaron is also accompanied with an introduction of local magnetism into an otherwise non-magnetic system. Magnetic moments of $0.945 \mu_B$ and $0.944 \mu_B$ were recorded for tetragonal and rhombohedral phases of BaTiO_3 . The reduction of normal Ti^{4+} to Ti^{3+} at polaronic site introduces an unpaired Ti-3d spin-polarized electron, resulting in magnetism that is highly concentrated at the polaronic site. Such polaron-induced magnetism in systems that are inherently ferroelectric opens up the possibility of multiferroism, which can be investigated in the future.

C. Effect of hole polarons on the ferroelectric properties

This section focuses on the impact of hole polarons on the ferroelectricity of tetragonal and rhombohedral polymorphs of BaTiO_3 . As observed for the case of electron polarons on tetragonal BaTiO_3 , the changes in the δ_{Fe} also displayed a planar dependence upon the formation of hole polarons. The tetragonal ferroelectric order was significantly affected in the octahedrons in the x-y plane containing polaronic oxygen. The modifications in the [001] δ_{Fe} were minimal for all sites in this plane, which was in contrast to from what was observed for the electron polaron described in the previous section. Owing to the shift of the two 1NN Ti atoms in the y-direction by 0.08 \AA , [010] polarization is induced in both the octahedrons. However, these dipole moments nullify each other as the shifts of these Ti atoms are opposite to each other, as shown in figure 7(a), and therefore do not contribute to the net polarization of the system. In addition, as shown in figure 7(a), polaronic distortions result in the surrounding O atoms in the x-y plane mov-

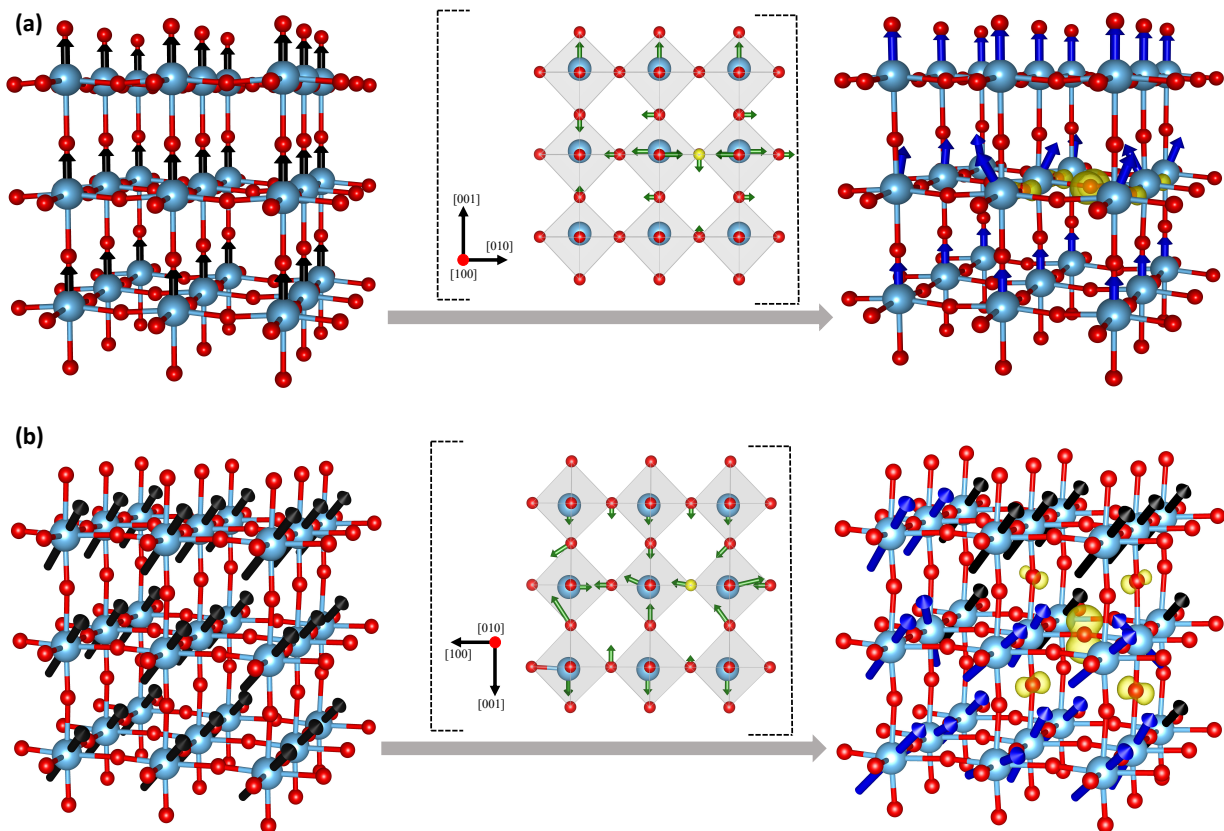


Figure 7. The figure represents a schematic depiction of the evolution of δ_{Fe} from a pristine to polaronic state as a hole localizes on an O atom in the (a) tetragonal and (b) rhombohedral phases of BaTiO_3 . The blue arrows in the figures on the right indicate the δ_{Fe} , which vary in both magnitude and direction compared to the δ_{Fe} in the pristine state, represented by black arrows. These transformations in the δ_{Fe} are attributed to the polaronic distortions, as represented in square brackets. Here, the yellow coloured atom represents the polaronic site and the green arrows depict the polaronic distortion

ing towards polaronic oxygen, likely due to the reduced electron-electron repulsion as the electron density is reduced on the polaronic oxygen. These shifts around the polaronic O atoms are approximately 0.02 \AA and are confined to the x-y plane. Consequently, we observed alterations in the FE order of the neighboring octahedrons in the x- and y-directions, introducing an additional negligible $[110]$ distortions across these sites. However, their contribution to the overall polarization is insignificant because for each site possessing this distortion, there is an equal and opposite distortion at another site in the same plane, resulting in dipole moments canceling each other out. The changes in δ_{Fe} are tabulated in Table S3 of the supplementary material. Overall, all x-y polarizations introduced to the sites in this specific plane by the hole polaron cancel out, whereas the changes in $[001]$ distortions are negligible.

For the x-y plane above the polaron, the Ti atoms showed increased off-centering by 0.011 \AA . Furthermore, the out-of-plane O atoms of the 2NN TiO_6 octahedra along the y-direction show distortion towards the polaronic oxygen, resulting in an increase in the length of the longer out-of-plane bond. The combined effect is an

increase of 6% in δ_{Fe} at sites belonging to this plane. Interestingly, the sites in the x-y plane below the polaron showed a negligible shift, resulting in only a minimal 3% decrease in δ_{Fe} . This discrepancy in both planes could potentially be due to the preexisting polarization direction. It is well established that the tetragonal distortion in BaTiO_3 involves a downward shift of the out-of-plane oxygen beneath (in the $[00\bar{1}]$ direction) Ti atom, creating a longer bond. We observed that for the octahedrons in the x-y plane above, the out-of-plane oxygen shifts inward towards the polaronic oxygen in the bottom plane, which goes hand-in-hand with the $[001]$ tetragonal distortion.

Our calculations revealed more complex alterations to δ_{Fe} upon the formation of hole polarons in the rhombohedral phase of BaTiO_3 . When hole polarons form on one of the in-plane O atoms of rhombohedral BaTiO_3 , we observed that the Ti atoms adjacent to this O atom undergo distortions, where the distortion is more pronounced on one Ti atom than on the other. In our study, the 1NN Ti atom in the $[100]$ direction exhibited a minimal shift of 0.013 \AA in the $[100]$ direction and a 0.01 \AA in the $[00\bar{1}]$ direction. However, the the 1NN Ti atom

in the $[\bar{1}00]$ direction showed a substantial distortion of 0.17 Å along the $[\bar{1}00]$ direction and a modest 0.01 Å distortion along the $[00\bar{1}]$ direction. Furthermore, polaronic O atom experienced a displacement of 0.039 Å along the $[100]$ direction. These distortions (schematically depicted in figure 7(b)) are responsible for the change in Ti-O bonds around the polaron, as discussed in section A. In addition, these distortions significantly affected the δ_{Fe} in the immediate vicinity and marginally in the farther sites. As mentioned earlier, there was a substantial shift in the $[\bar{1}00]$ 1NN Ti atom, which was sufficiently pronounced to result in the reversal of the polarization in the x-direction at this site. We observed a 50% reduced negative δ_{Fe} , while the δ_{Fe} also experienced a minimal 5% decrease in the z-direction for this specific site. The 1NN TiO_6 octahedron in the $[100]$ direction exhibited modest modifications in the x-direction δ_{Fe} with a 10% decrease. In addition, the y- and z-direction δ_{Fe} were modified, as tabulated in Table S4. For the 2NN octahedron in the $[100]$ direction, the Ti atom distorted by 0.05 Å towards its centrosymmetric position only along the x-direction, consequently resulting in a significant 74% reduction of the x-direction δ_{Fe} . Although modest, there was also a 4% increase in the y- and z-direction δ_{Fe} for this specific octahedron.

Despite the significant changes in δ_{Fe} primarily concentrated on the octahedrons along the x-direction compared to other sites, less pronounced shifts were still observed for other sites. We observed that the 2NN along the y and z directions showed a clear pattern in δ_{Fe} modifications, which is correlated with the inherent $[111]$ rhombohedral polarization. For the 2NN octahedrons along the directions aligned with a component of the $[111]$ polarization, specifically the 2NN TiO_6 octahedrons along the $[010]$ direction aligned with the y component, and the $[001]$ direction aligned with the z component, there was a more pronounced change in the δ_{Fe} . In the $[010]$ direction, a 17% increase in the y-direction δ_{Fe} was experienced by one site, whereas a 12% decrease was observed in the other. Similarly, both 2NN TiO_6 octahedra in the $[001]$ direction experienced a 14% decrease in the z-direction δ_{Fe} . In contrast, for the 2NN along the opposite direction of the polarization component ($[0\bar{1}0]$ and $[00\bar{1}]$), the modifications to the δ_{Fe} were negligible. Therefore, our results indicate that inherent polarization plays a critical role in shaping the distortion pattern around the polaron, thereby affecting δ_{Fe} . It appears that the atoms aligned with the direction of inherent polarization is more susceptible to transformations relative to those on the opposite side. Although the specific distortion

patterns are different, these observations are similar to the case of electron polarons in rhombohedral BaTiO_3 .

Consistent with our approach to electron polaron systems, we also calculated P_s for hole polaron systems. Our calculations revealed a negligible effect on the overall P_s of the tetragonal phase of BaTiO_3 , which was determined to be 0.395 C/cm². For the polaronic rhombohedral system, the calculations revealed a slight increase from 0.45 C/cm² (quantified for pristine BaTiO_3) to 0.46 C/cm². Furthermore, the energy difference between the ferroelectric and paraelectric polaronic states was calculated for both phases of BaTiO_3 and compared with that of pristine systems. These studies have reported a value of 0.035 eV/f.u. for tetragonal BaTiO_3 , which is comparable to that of the pristine states. For the rhombohedral phase, the energy difference between the polaronic states was quantified to be 0.038 eV/f.u.. Due to the formation of polarons, the hole polaron systems also revealed the presence of local magnetic moments of 0.920 μ_B , 0.926 μ_B and 0.912 μ_B respectively for the cubic, tetragonal and rhombohedral phases.

IV. CONCLUSION

This study looked into the interplay between ferroelectricity and polaron formation in the cubic, tetragonal and rhombohedral phases of BaTiO_3 . The studies reveal the stability of polaronic solution for both hole and electron polarons across all the three polymorphs of BaTiO_3 . Interestingly, the Ti off-centering plays a significant role in stabilizing the electron polaron formed on the Ti site for the ferroelectric phases of BaTiO_3 , while such an effect is not observed for hole polarons trapped on an oxygen site. Although there is only a negligible effect on overall net polarization, a slight reduction to the spontaneous polarization for the electron polaron systems and a slight increase in the hole polaron system is noticed. Since the formation of polarons is accompanied with a magnetic moment, there is a co-existence of ferroelectricity and magnetism in the systems. These findings could pave way for further optimization, potentially leading to multiferroicity in the ferroelectric phases of BaTiO_3 .

V. REFERENCES

-
- [1] W. Cochran, Crystal stability and the theory of ferroelectricity, *Advances in Physics* **9**, 387 (1960).
 [2] R. E. Cohen, Origin of ferroelectricity in perovskite oxides, *Nature* **358**, 136 (1992).

- [3] G. A. Samara, Ferroelectricity revisited—advances in materials and physics, in *Solid State Physics*, Vol. 56 (Elsevier, 2001) pp. 239–458.
- [4] R. King-Smith and D. Vanderbilt, Theory of polarization of crystalline solids, *Physical Review B* **47**, 1651 (1993).
- [5] M. E. Lines and A. M. Glass, *Principles and applications of ferroelectrics and related materials* (Oxford university press, 2001).
- [6] J. Scott, Applications of modern ferroelectrics, *science* **315**, 954 (2007).
- [7] K. M. Rabe, C. H. Ahn, and J.-M. Triscone, *Physics of ferroelectrics: a modern perspective*, Vol. 105 (Springer Science & Business Media, 2007).
- [8] G. Kwei, A. Lawson, S. Billinge, and S. Cheong, Structures of the ferroelectric phases of barium titanate, *The Journal of Physical Chemistry* **97**, 2368 (1993).
- [9] S. Piskunov, E. Heifets, R. Eglitis, and G. Borstel, Bulk properties and electronic structure of SrTiO_3 , BaTiO_3 , PbTiO_3 perovskites: an ab initio hf/dft study, *Computational Materials Science* **29**, 165 (2004).
- [10] J. Chen, M. P. Harmer, and D. M. Smyth, Compositional control of ferroelectric fatigue in perovskite ferroelectric ceramics and thin films, *Journal of applied physics* **76**, 5394 (1994).
- [11] X. Lou, Polarization fatigue in ferroelectric thin films and related materials, *Journal of Applied Physics* **105** (2009).
- [12] S. Qiu and H. Fu, Extended planar defects of oxygen vacancies in ferroelectric BaTiO_3 and impact on ferroelectricity, *Scientific Reports* **13**, 19578 (2023).
- [13] J. Wang, Y. Shen, F. Song, F. Ke, Y. Bai, and C. Lu, Effects of oxygen vacancies on polarization stability of barium titanate, *Science China Physics, Mechanics & Astronomy* **59**, 1 (2016).
- [14] V. F. Michel, T. Esswein, and N. A. Spaldin, Interplay between ferroelectricity and metallicity in BaTiO_3 , *Journal of Materials Chemistry C* **9**, 8640 (2021).
- [15] S. Das, R. Mishra, and B. Roul, Magnetic and ferroelectric properties of ni doped BaTiO_3 , *Solid state communications* **191**, 19 (2014).
- [16] K. Klyukin and V. Alexandrov, Effect of intrinsic point defects on ferroelectric polarization behavior of SrTiO_3 , *Physical Review B* **95**, 035301 (2017).
- [17] D. Lee, H. Lu, Y. Gu, S.-Y. Choi, S.-D. Li, S. Ryu, T. Paudel, K. Song, E. Mikheev, S. Lee, *et al.*, Emergence of room-temperature ferroelectricity at reduced dimensions, *Science* **349**, 1314 (2015).
- [18] M. Choi, F. Oba, and I. Tanaka, Role of ti antisitelike defects in SrTiO_3 , *Physical review letters* **103**, 185502 (2009).
- [19] S. Ning, A. Kumar, K. Klyukin, E. Cho, J. H. Kim, T. Su, H.-S. Kim, J. M. LeBeau, B. Yildiz, and C. A. Ross, An antisite defect mechanism for room temperature ferroelectricity in orthoferrites, *Nature Communications* **12**, 4298 (2021).
- [20] R. Materlik, C. Künneth, M. Falkowski, T. Mikolajick, and A. Kersch, Al-, y-, and la-doping effects favoring intrinsic and field induced ferroelectricity in HfO_2 : A first principles study, *Journal of Applied Physics* **123** (2018).
- [21] M. H. Park, D. H. Lee, K. Yang, J.-Y. Park, G. T. Yu, H. W. Park, M. Materano, T. Mittmann, P. D. Lomenzo, T. Mikolajick, *et al.*, Review of defect chemistry in fluorite-structure ferroelectrics for future electronic devices, *Journal of Materials Chemistry C* **8**, 10526 (2020).
- [22] A. S. Alexandrov and J. T. Devreese, *Advances in polaron physics*, Vol. 159 (Springer, 2010).
- [23] L. D. Landau, Über Die Bewegung der Elektronen in Kristallgitter, *Phys. Z. Sowjetunion* **3**, 644 (1933).
- [24] D. Emin, *Polarons* (Cambridge University Press, 2013).
- [25] C. Franchini, M. Reticioli, M. Setvin, and U. Diebold, Polarons in materials, *Nature Reviews Materials* **6**, 560 (2021).
- [26] W. H. Sio, C. Verdi, S. Poncé, and F. Giustino, Polarons from first principles, without supercells, *Physical Review Letters* **122**, 246403 (2019).
- [27] T. Holstein, Studies of polaron motion: Part ii. the “small” polaron, *Annals of physics* **8**, 343 (1959).
- [28] M. Reticioli, U. Diebold, G. Kresse, and C. Franchini, Small polarons in transition metal oxides, *Handbook of Materials Modeling: Applications: Current and Emerging Materials*, 1035 (2020).
- [29] P. Nagels, M. Denayer, and J. Devreese, Electrical properties of single crystals of uranium dioxide, *Solid State Communications* **1**, 35 (1963).
- [30] C. Crevecoeur and H. De Wit, Electrical conductivity of li doped MnO , *Journal of Physics and Chemistry of Solids* **31**, 783 (1970).
- [31] A. Stoneham, J. Gavartin, A. Shluger, A. Kimmel, D. M. Ramo, H. Rønnow, G. Aeppli, and C. Renner, Trapping, self-trapping and the polaron family, *Journal of Physics: Condensed Matter* **19**, 255208 (2007).
- [32] A. Zhugayevych and S. Tretiak, Theoretical description of structural and electronic properties of organic photovoltaic materials, *Annual Review of Physical Chemistry* **66**, 305 (2015).
- [33] V. Coropceanu, J. Cornil, D. A. da Silva Filho, Y. Olivier, R. Silbey, and J.-L. Brédas, Charge transport in organic semiconductors, *Chemical reviews* **107**, 926 (2007).
- [34] S. Roth and D. Carroll, *Foundations of Solid State Physics: Dimensionality and Symmetry* (John Wiley & Sons, 2019).
- [35] K. Hinrichs and K.-J. Eichhorn, *Ellipsometry of functional organic surfaces and films*, Vol. 52 (Springer, 2018).
- [36] A. De Sio, F. Troiani, M. Maiuri, J. Réhault, E. Sommer, J. Lim, S. F. Huelga, M. B. Plenio, C. A. Rozzi, G. Cerullo, *et al.*, Tracking the coherent generation of polaron pairs in conjugated polymers, *Nature communications* **7**, 13742 (2016).
- [37] A. Kaminski and S. D. Sarma, Polaron percolation in diluted magnetic semiconductors, *Physical Review Letters* **88**, 247202 (2002).
- [38] J. d. Teresa, M. Ibarra, P. Algarabel, C. Ritter, C. Marquina, J. Blasco, J. Garcia, A. del Moral, and Z. Arnold, Evidence for magnetic polarons in the magnetoresistive perovskites, *Nature* **386**, 256 (1997).
- [39] A. Daoud-Aladine, J. Rodriguez-Carvajal, L. Pinsard-Gaudart, M. Fernandez-Diaz, and A. Revcolevschi, Zener polaron ordering in half-doped manganites, *Physical review letters* **89**, 097205 (2002).
- [40] J.-S. Zhou and J. Goodenough, Zener versus de gennes ferromagnetism in $\text{La}_{1-x}\text{Sr}_x\text{MnO}_3$, *Physical Review B* **62**, 3834 (2000).
- [41] D. Cortecchia, J. Yin, A. Bruno, S.-Z. A. Lo, G. G. Gurzadyan, S. Mhaisalkar, J.-L. Brédas, and C. Soci, Polaron self-localization in white-light emitting hybrid perovskites, *Journal of Materials Chemistry C* **5**, 2771

- (2017).
- [42] M. Kang, S. W. Jung, W. J. Shin, Y. Sohn, S. H. Ryu, T. K. Kim, M. Hoesch, and K. S. Kim, Holstein polaron in a valley-degenerate two-dimensional semiconductor, *Nature materials* **17**, 676 (2018).
- [43] J. Nelson, J. J. Kwiatkowski, J. Kirkpatrick, and J. M. Frost, Modeling charge transport in organic photovoltaic materials, *Accounts of chemical research* **42**, 1768 (2009).
- [44] M. Reticcioli, M. Setvin, X. Hao, P. Flauger, G. Kresse, M. Schmid, U. Diebold, and C. Franchini, Polaron-driven surface reconstructions, *Physical Review X* **7**, 031053 (2017).
- [45] M. Reticcioli, I. Sokolović, M. Schmid, U. Diebold, M. Setvin, and C. Franchini, Interplay between adsorbates and polarons: Co on rutile TiO_2 (110), *Physical Review Letters* **122**, 016805 (2019).
- [46] A. Millis, R. Mueller, and B. I. Shraiman, Fermi-liquid-to-polaron crossover. ii. double exchange and the physics of colossal magnetoresistance, *Physical Review B* **54**, 5405 (1996).
- [47] C. Verdi, F. Caruso, and F. Giustino, Origin of the crossover from polarons to fermi liquids in transition metal oxides, *Nature Communications* **8**, 15769 (2017).
- [48] K. Miyata, D. Meggiolaro, M. T. Trinh, P. P. Joshi, E. Mosconi, S. C. Jones, F. De Angelis, and X.-Y. Zhu, Large polarons in lead halide perovskites, *Science advances* **3**, e1701217 (2017).
- [49] K. Miyata and X.-Y. Zhu, Ferroelectric large polarons, *Nature materials* **17**, 379 (2018).
- [50] E. Ghorbani, L. Villa, P. Erhart, A. Klein, and K. Albe, Self-consistent calculations of charge self-trapping energies: A comparative study of polaron formation and migration in PbTiO_3 , *Physical Review Materials* **6**, 074410 (2022).
- [51] M. Aguilar, C. Gonzalo, and G. Godefroy, X-ray induced luminescence from BaTiO_3 , *Solid State Communications* **30**, 525 (1979).
- [52] H. Ihrig, J. Hengst, and M. Klerk, Conductivity-dependent cathodoluminescence in BaTiO_3 , SrTiO_3 and TiO_2 , *Zeitschrift für Physik B Condensed Matter* **40**, 301 (1981).
- [53] J. Boyeaux and F. Michel-Calendini, Small polaron interpretation of BaTiO_3 transport properties from drift mobility measurements, *Journal of Physics C: Solid State Physics* **12**, 545 (1979).
- [54] E. Iguchi, N. Kubota, T. Nakamori, N. Yamamoto, and K. Lee, Polaronic conduction in n-type BaTiO_3 doped with La^{2+} or Gd^{2+} , *Physical Review B* **43**, 8646 (1991).
- [55] H. Ihrig and D. Hennings, Electrical transport properties of n-type BaTiO_3 , *Physical Review B* **17**, 4593 (1978).
- [56] X. Jing, W. Xu, C. Yang, J. Feng, A. Zhang, Y. Zeng, M. Qin, M. Zeng, Z. Fan, J. Gao, *et al.*, Tuning electrical conductivity, charge transport, and ferroelectricity in epitaxial BaTiO_3 films by nb-doping, *Applied Physics Letters* **110** (2017).
- [57] W. Traiwattanapong, A. Janotti, N. Umezawa, S. Limpitjumnong, P. Reunchan, *et al.*, Self-trapped holes in BaTiO_3 , *Journal of Applied Physics* **124** (2018).
- [58] P. Erhart, A. Klein, D. Åberg, and B. Sadigh, Efficacy of the $\text{dft}+u$ formalism for modeling hole polarons in perovskite oxides, *Physical Review B* **90**, 035204 (2014).
- [59] T. Xu, M. Mori, H. Hirakata, T. Kitamura, and T. Shimada, Emergent ultrasoft multiferroics in paraelectric perovskite oxide by hole polarons, *Physical Chemistry Chemical Physics* **26**, 842 (2024).
- [60] N. Tsunoda, Y. Kumagai, and F. Oba, Stabilization of small polarons in BaTiO_3 by local distortions, *Physical Review Materials* **3**, 114602 (2019).
- [61] T. Xu, T. Shimada, Y. Araki, M. Mori, G. Fujimoto, J. Wang, T.-Y. Zhang, and T. Kitamura, Electron engineering of metallic multiferroic polarons in epitaxial BaTiO_3 , *npj Computational Materials* **5**, 23 (2019).
- [62] N. U. Din, T. Jiang, S. Gholam-Mirzaei, M. Chini, and V. Turkowski, Electron-electron correlations and structural, spectral and polarization properties of tetragonal BaTiO_3 , *Journal of Physics: Condensed Matter* **32**, 475601 (2020).
- [63] G. Gebreyesus, L. Bastonero, M. Kotiuga, N. Marzari, and I. Timrov, Understanding the role of hubbard corrections in the rhombohedral phase of BaTiO_3 , *Physical Review B* **108**, 235171 (2023).
- [64] P. Hohenberg and W. Kohn, Inhomogeneous electron gas, *Physical review* **136**, B864 (1964).
- [65] E. K. Gross and R. M. Dreizler, *Density functional theory*, Vol. 337 (Springer Science & Business Media, 2013).
- [66] J. L. Gavartin, P. V. Sushko, and A. L. Shluger, Modeling charge self-trapping in wide-gap dielectrics: Localization problem in local density functionals, *Physical review B* **67**, 035108 (2003).
- [67] B. Sadigh, P. Erhart, and D. Åberg, A variational polaron self-interaction corrected total-energy functional for charge excitations in wide-band gap insulators, *arXiv preprint arXiv:1401.7137* (2014).
- [68] V. I. Anisimov, J. Zaanen, and O. K. Andersen, Band theory and mott insulators: Hubbard u instead of stoner i , *Physical Review B* **44**, 943 (1991).
- [69] S. L. Dudarev, G. A. Botton, S. Y. Savrasov, C. Humphreys, and A. P. Sutton, Electron-energy-loss spectra and the structural stability of nickel oxide: An $\text{LSDA}+u$ study, *Physical Review B* **57**, 1505 (1998).
- [70] A. V. Krugau, O. A. Vydrov, A. F. Izmaylov, and G. E. Scuseria, Influence of the exchange screening parameter on the performance of screened hybrid functionals, *The Journal of chemical physics* **125** (2006).
- [71] J. Heyd, G. E. Scuseria, and M. Ernzerhof, Hybrid functionals based on a screened coulomb potential, *The Journal of chemical physics* **118**, 8207 (2003).
- [72] G. Kresse and J. Furthmüller, Efficient iterative schemes for ab initio total-energy calculations using a plane-wave basis set, *Physical review B* **54**, 11169 (1996).
- [73] J. P. Perdew, K. Burke, and M. Ernzerhof, Generalized gradient approximation made simple, *Physical review letters* **77**, 3865 (1996).
- [74] G. Kresse and D. Joubert, From ultrasoft pseudopotentials to the projector augmented-wave method, *Physical review b* **59**, 1758 (1999).
- [75] P. E. Blöchl, Projector augmented-wave method, *Physical review B* **50**, 17953 (1994).
- [76] H. F. Kay and P. Vousden, Xcv. symmetry changes in barium titanate at low temperatures and their relation to its ferroelectric properties, *The London, Edinburgh, and Dublin Philosophical Magazine and Journal of Science* **40**, 1019 (1949).
- [77] G. Shirane and A. Takeda, Transition energy and volume change at three transitions in barium titanate, *Journal of the Physical Society of Japan* **7**, 1 (1952).

- [78] R. Resta and D. Vanderbilt, Theory of polarization: a modern approach, in *Physics of ferroelectrics: a modern perspective* (Springer, 2007) pp. 31–68.